
Article:
Chomtong, P. orcid.org/0000-0002-4620-6413, Krachodnok, P. orcid.org/0000-0002-5300-342X, Konpang, J. et al. (3 more authors) (2024) Miniaturized Multiband EBG Reflector Using DICPW Structure for Wireless Communication Systems. IEEE Access. ISSN 2169-3536

https://doi.org/10.1109/access.2024.3369477

IEEE Access
Multidisciplinary | Rapid Review | Open Access Journal

Date of publication xxxx 00, 0000, date of current version xxxx 00, 0000.

Digital Object Identifier 10.1109/ACCESS.2022.Doi Number

Miniaturized Multiband EBG Reflector Using DICPW Structure for Wireless Communication Systems

P. Chomtong[1], Member, IEEE, P. Krachodnok[2], Member, IEEE, J. Konpang[3], Member, IEEE , N. Somjit[4,5,6], Senior Member, IEEE, C. Mahatthanajatuphat[7] Member, IEEE and P. Akkaraekthalin[7], Member, IEEE

[1]Department of Teacher Training in Electrical Engineering, Faculty of Technical Education, King Mongkut's University of Technology NorthBangkok, Thailand.
[2]School of Telecommunication Engineering, Institute of Engineering, Suranaree University of Technology, Nakhon Ratchasima, Thailand.
[3]Department of Electrical and Telecommunication Engineering, Faculty of Engineering, Rajamangala University of Krungthep, Thailand.
[4]School of Electronic and Electrical Engineering, University of Leeds, Leeds, U.K.
[5]Division of Micro and Nanosystems (MST), KTH Royal Institute of Technology, Malvinas väg 10 SE-100 Stockholm Sweden
[6]Department of Electrical Engineering, Faculty of Engineering, Chiang Mai University, 239 Huay Kaew Road, Muang District, Chiang Mai, Thailand.
[7]Department of Electrical and Computer Engineering, Faculty of Engineering, King Mongkut's University of Technology North, Bangkok, Thailand

Corresponding author: P. Krachodnok (e-mail: priam@sut.ac.th). Co-Corresponding author: J. Konpang (jessada.k@mail.rmutk.ac.th)

This work was supported by King Mongkut's University of Technology North Bangkok contract no. KMUTNB-65-know-31, and in part by the Engineering and Physical Science Research Council under Grant EP/S016813/1, and the Swedish Research Council (VR) under Grant 2021-05842_VR.

ABSTRACT Wireless communication technology evolves to meet current needs, focusing on antenna size reduction for smaller, multi-frequency devices. This research introduces a novel approach to miniaturizing a multiband Electromagnetic Band Gap (EBG) reflector using a Double Interdigitated Coplanar Waveguide (DICPW) structure. The mushroom-patterned EBG unit cell, employing a double interdigital technique based on a Coplanar Waveguide (CPW), achieves a significantly slower wave on the transmission line. The unit cell size can be reduced from λ/2 to λ/8, allowing control over the second to fourth resonance frequencies. Engineered for a fundamental frequency of 1.8 GHz (LTE), the proposed EBG unit cell supports frequency ranges of 2.45 GHz (WLAN), 4.3 GHz (Altimeter), and 5.2 GHz (WLAN). Integrating this EBG reflector with a dipole antenna at the same frequency results in directional radiation patterns and gains of 8.29 dBi, 8.76 dBi, 8.55 dBi, and 8.22 dBi at resonance frequencies. The innovative reflector, with improved gain and compact dimensions, is relevant to cube satellite and wireless communication systems with versatile multiband frequency requirements.

INDEX TERMS Interdigital, Multi band, Electromagnetic Band Gap, EBG reflector, Coplanar Waveguide, ICPW, Capacitive load.

I. INTRODUCTION

Wireless communication technology is in a constant state of evolution to meet contemporary application needs. Extensive research aims to enhance data transmission efficiency over longer distances and reduce the size of communication equipment. Antennas play a crucial role in these systems, prompting research to develop antennas capable of responding to various characteristics, including multi-frequency support, smaller size, higher gain, and controlled propagation direction [1-3]. Despite advances, there are limitations. Antennas with multi-frequency responses may exhibit uneven radiation patterns at harmonic frequencies. Traditional reflectors enhance gain but lose energy, limiting wave propagation. Array approaches can achieve high gains but involve challenging antenna matching [4], [5].

To address these challenges, a novel material known as metamaterial has been developed [6], [7]. Metamaterial is defined as a macroscopic composite with a synthetic and periodic architecture designed to produce an optimized combination not available in nature. Metamaterials can be used to obtain negative permeability and positive permittivity, vice versa, or both negative or both positive (in all possible combinations). The utilization of

metamaterial structures offers advantages in communication electronic components, such as antennas and filters.

This results in unique properties when used as an antenna reflector [8-10], improving the antenna's gain rate compared to a conventional reflector of the same size. Moreover, when employed as a director [11], it can facilitate transmission in the desired frequency band and enhance the antenna's gain. Additionally, it is suitable for use as an antenna shield against the environment, with minimal interference or energy loss for propagation. Various metamaterial design techniques, such as frequency-selective surface (FSS) [12-16], involve creating materials with specified transmittance properties or the ability to reflect a specific frequency range. In addition, there is a metamaterial design technique called EBG [17-27] that is utilized as an antenna reflector. EBG structures are defined as periodic objects capable of preventing the propagation of all electromagnetic waves within a specified frequency band for all incident angles and polarization states [28-31]. The characteristics of an EBG are similar to those of an Artificial Magnetic Conductor (AMC) [32-37]. Both structures are designed to manipulate electromagnetic waves, but they serve different purposes and operate on different principles. AMC is designed to mimic the behavior of a perfect magnetic conductor at a specific frequency by using a magnetic wall principle to reflect electromagnetic waves. It achieves this by increasing the impedance on the surface of a planar material. On the other hand, the EBG structure is designed to create a forbidden band of frequencies where the propagation of electromagnetic waves is prohibited. EBG controls the current in the gap and the absence of current on the surface of the material over a specified frequency range [38]-[39]. Thus, when an electromagnetic wave impacts the reflector created using these approaches, it results in a higher antenna gain compared to a conventional reflector with an EBG reflector. Alternatively, passive circuits such as Cavity [40] can be designed using EBG to enhance transmission efficiency compared to conventional materials. Among the aforementioned material design methodologies, there are continuous improvements. These include the ability for the frequency response to be utilized over a wide range of frequencies in the same material, a reduction in the material's size, and cost-effectiveness, enabling its application to increase the efficiency of various communication systems. Nevertheless, creating material that can respond to a wide range of frequencies with small dimensions remains a significant challenge.

To explore these concepts further, a miniaturized multiband EBG reflector utilizing a Double Interdigitated Coplanar Waveguide (DICPW) structure is proposed for wireless communication systems. The DICPW technique significantly enhances capacitance and allows for better control of resonance frequencies. The EBG unit cell,

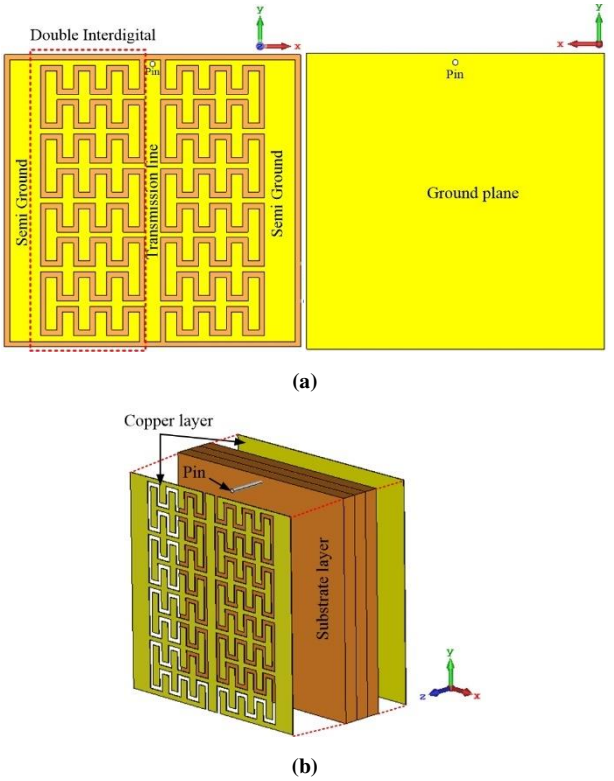

FIGURE 1. The configuration of proposed EBG unit cell structure (a) front and back layer of EBG unit cell and (b) copper layer and substrate layer of EBG unit cell with a pin.

developed on a printed circuit board, demonstrates improved gain and frequency control. A unit cell EBG is based on the fundamental structure of the CPW [41-44]. Generally, the traditional CPW structure creates the capacitances between the transmission line and the ground, which are extremely modest and do not impact the fundamental frequency resonance with harmonic frequency. By raising the capacitance value between the transmission line and ground using the interdigital technique, also known as ICPW [45-48], the resonance frequency shift of the harmonic frequencies can be regulated according to the desired frequency range, with no change in the resonant frequency of the fundamental frequency, and a dispersion range without surface waves covering the required frequency range can be generated. In addition, raising the capacitance value using ICPW approach may reduce the size of the unit cell to less than $\lambda/4$, and when the unit cell is arranged in an array to be used as an antenna reflector, it can improve the gain compared to a conventional reflector. Due to structural limits, however, the capacitive value of ICPW can only be raised to a limited amount, and the regulation of harmonic frequencies to produce the phase shift and resonance frequencies are not achievable over multiple frequencies. In order to circumvent these restrictions, the unit cell was created with the capability of increasing capacitance even more. The DICPW is based on a unit cell structure with

mushroom properties, which significantly enhances the capacitance value created by the finger between the transmission line and the finger of the ground plane. This immediately influences the frequency control of second to fourth-order resonant frequencies and provides the desired resonant frequency by raising or reducing the capacitance in combination with the transmission line's size. The application of that approach will result in a substantial slow-wave impact [49-52] on the structure, resulting in uneven electrical and physical lengths as well as a $\lambda/8$ reduction in the unit cell size of EBG. Raising the capacitance value is analogous to attaching a capacitor to the transmission cable's end, which results in the phenomena of unit cell size reduction.

From the EBG reflector technique design as presented above the use of DICPW technique on the EBG unit cell structure can significantly increase the double capacitive load, which results in a greater slow-wave effect on the transmission line than with the conventional capacitive load increase technique. This also means that the electrical length of the transmission line does not match its physical length. To equalize both, the physical length must be reduced. The DICPW technique can reduce the physical length to as low as $\lambda/8$ of the original length. In addition, by adjusting the value of the double capacitive load, the second to fourth resonance frequencies can be controlled to resonate at the desired frequency range. Drilling pins on the EBG unit cell structure will cause the resonance frequency range to change phase in an S-curve shape and be free of surface waves, with only wave propagation. When exposed to energy in the aforementioned resonance frequency range, it will have better reflection properties than ordinary materials. This clearly shows that the designed EBG unit cell is very small in size, responds to a multi of frequencies, and has better reflection properties than conventional reflectors. When the EBG unit cells are connected in an array to form an EBG reflector, the number of EBG unit cells can be freely adjusted to accommodate a variety of antenna types and frequency ranges. This is because the EBG unit cells are very small in size and respond in a multi-band manner. As a consequence, the reflector created using this method will aid the antenna in achieving a greater gain than would be possible with a normal reflector. It is compact, lightweight, and has a straightforward design.

This research introduces an innovative approach to EBG reflector design, addressing challenges posed by traditional antennas and reflectors. The proposed DICPW technique exhibits promise in achieving a multi-frequency response, size reduction, and enhanced performance, making it applicable to various wireless communication systems. The EBG reflector design presented in this article includes the EBG unit cell design discussed in Section II. This section details the application of the DICPW technique to reduce the structure's size and control resonant frequencies, resulting in a multi-band response. Section III involves EBG simulation, providing insights into the operation of the EBG unit cell and reflector when connected to dipole and loop antennas, testing their performance in increasing antenna gain. Section IV delves into measurements and results, describing the performance of the constructed EBG reflector. Lastly, Section V concludes the research by summarizing findings and presenting suggestions for future research.

II. DESIGN OF THE EBG UNIT CELL

This section presents a design for an EBG unit cell in the shape of a mushroom [17-20] with a pin connection between the transmission line and the ground plane. The structure does not function as an electromagnetic bandgap but rather as an artificial magnetic conductor [32]. The mushroom structure achieves a high-impedance surface capable of creating an artificial magnetic ground plane, which increases antenna gain while maintaining compact dimensions. The EBG unit cell structure is based on CPW [41-44], enhancing the capacitance between the transmission line and the semi-ground. Figs. 1(a) and 1(b) depict the proposed EBG unit cell structure using the double interdigital technique. This method exhibits higher capacitance compared to the conventional interdigital method [47-50]. The capacitive value of the interdigital method is typically produced by the finger between the transmission line and the semi-ground [26], [27] but the double interdigital technique adds an extra finger to the semi-ground, leading to a significant increase in the capacitive value between the transmission line and the semi ground on the unit cell structure. In evaluating the structure of the proposed unit cell depicted in Fig. 2(a), which derives its fundamental structure from CPW, the CPW structure serves as a point of reference. Capacitances generated by the proposed unit cell structure could be categorized as follows: C_i is the capacitance created by the finger and gap between the transmission line and the semi-ground, C_{is} is the capacitance generated by the finger in the semi-ground, C_f is the fringe capacitance, C_i' is the capacitance produced by the substrate between the transmission line and the semi ground, and C_g is capacitance in the substrate layer formed between the transmission line with ground plane and the semi ground with the ground plane. The width of the transmission line is denoted by parameter A, while the distance between the semi-ground is denoted by parameter B. C_D is the capacitance of the double interdigital structure arising from the combination of C_i and C_{is} in the unit cell structure of EBG, as shown in Fig. 2(b). It was discovered that the significant capacitive impact on the regulation of the second and fourth resonant frequencies is a result of the combination of C_g and C_D on the structure. The capacitance values C_f and C_i' are extremely tiny, and hence have a negligible impact on the EBG unit cell structure's resonance frequency. R' is the transmission line's loss, and h is the substrate's height. Increasing the number of layers to three will increase the phase width in the S-curve to accommodate the appropriate frequency without surface waves. Fig. 2(c) depicts

the equivalent circuit of the unit cell structure where *TP* is the transmission line part divided into three parts: TP_1 and TP_3 are the transmission line sections with capacitance C_i, and TP_2 is the transmission line with capacitance C_D, which results from the combination of capacitance C_i and C_{is}. In the event that the transmission line parts of EBG unit cell in proposed is same in all sections. Total conductor impedance (Z_t) equals $Z_t = Z_a = Z_b = Z_c$, total propagation constant (β_t) equals $\beta_t = \beta_a = \beta_b = \beta_c$, and total electrical length (θ_t) equals $\theta_t = \theta_a = \theta_b = \theta c$. From the equivalent circuit, it can be observed that the transmission lines are connected to the capacitive C_i, C_{is}, and C_g, which have a significant impact on the EBG unit cell structure. The connection is characterized by a capacitive connection at the transmission line's end, which generates a large slow wave on the transmission line and causes the electrical length (θ_t) to differ from the transmission line's physical length. Consequently, it is possible to reduce the physical size of an EBG unit cell from $\lambda/2$ to $\lambda/8$ at 1.8 GHz [26], [31], [46-49], and the connecting pin between the transmission line and ground plane can remove surface waves on the structure and induce an inductance (L). In the EBG unit cell structure, it is discovered that jX_L is lower than $-jX_C$; hence, the total capacitive circuit (C_t) impacts the entire resonance frequency. The capacitive parameters in the EBG unit cell structure may be derived using the equation below.

$$C_t = C_D + C_i' + C_g + C_f' \tag{1}$$

When

$$C_D = C_i + C_{is}$$

$$C_i = \frac{(\varepsilon_r + 1)}{L_t} L_f (\varepsilon_r + 1)\left(0.1(n-3) + 0.11\right)$$

$$C_{is} = \frac{(\varepsilon_r + 1)}{L_t'} L_f' (\varepsilon_r + 1)\left(0.1(n'-3) + 0.11\right)$$

$$C_i' = \frac{\varepsilon_0 \varepsilon_r}{\pi} \ln\left[\cot h\left(\frac{\pi}{4}\frac{B}{h}\right)\right] + 0.65 c_f \left(\frac{0.02}{B/h} + 1 - \frac{1}{\varepsilon_0^2}\right)$$

$$C_g = \varepsilon_0 \varepsilon_r \frac{A}{h}$$

$$C_f = \frac{\sqrt{\varepsilon_r}}{(C_D) - (C_g)}$$

According to (1), the details of the equation are as follows: L_t and L_t' represent the entire length of the interdigital in the transmission line and the semi-ground section, respectively. L_f indicates the finger length between the transmission line and the semi-ground part. L_f' denotes the finger length in the semi-ground section. n and n' indicate the total number of fingers. When K is the entire elliptic integral of the first kind [10], [26], [44] the total impedance of a transmission line (Z_t) may be determined by applying the (2).

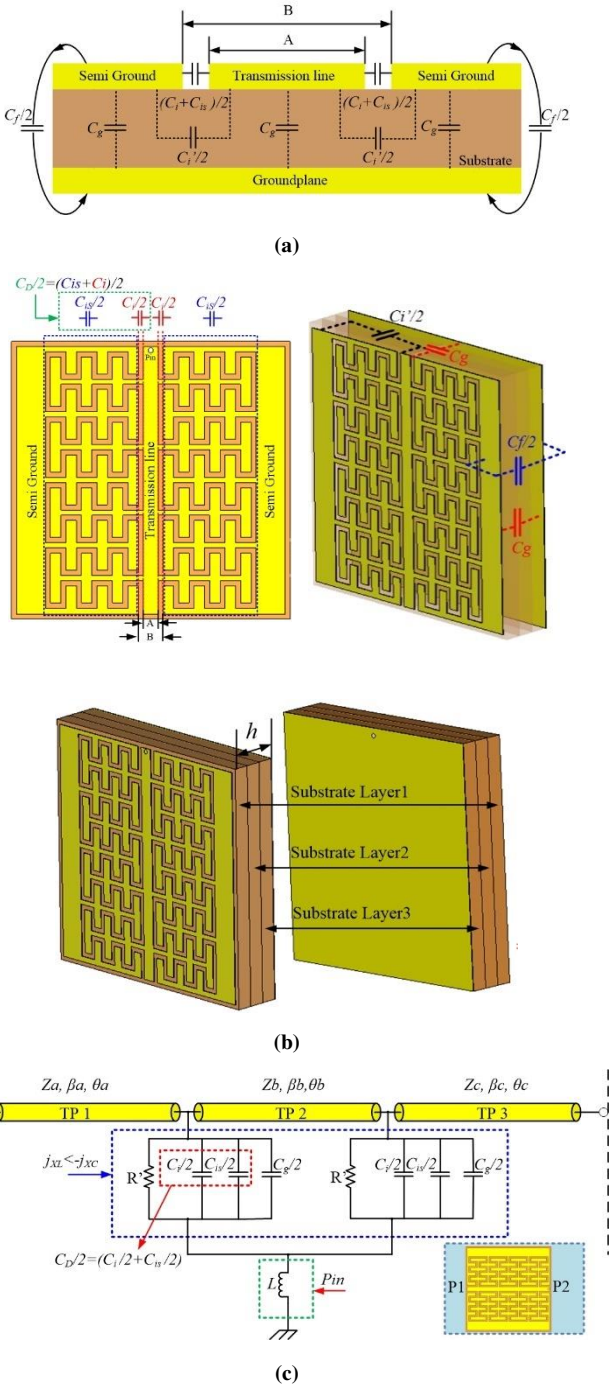

FIGURE 2. **The proposed unit cell and parameters of the equivalent circuit in (a) cross section layer, (b) Font and side view, and (c) equivalent circuit of the unit cell structure.**

$$Z_t = \frac{60\pi}{\sqrt{\varepsilon_{eff}}} \frac{1}{\frac{K(k)}{K(k')} + \frac{K(k_x)}{K(k_x')}} \tag{2}$$

When

$$\varepsilon_{eff} = \left[1.0 +_r \frac{K(k')}{K(k)} \frac{K(k_x)}{K(k'_x)} \Big/ 1.0 + \frac{K(k')}{K(k)} \frac{K(k'_x)}{K(k_x)} \right]$$

$$k = \frac{A}{B}, k' = \sqrt{1.0 - k^2}$$

$$k_x = \tanh\left(\frac{\pi A}{2h}\right) \Big/ \tanh\left(\frac{\pi B}{2} h\right), k'_x = \sqrt{1.0 - k_x^2}$$

$$\beta = \frac{2\pi}{\lambda}$$

Using (1) and (2), the electrical length of transmission line at the first through fourth resonance frequency may be computed using (3). The electrical lengths θ_{a0}, θ_{a1}, θ_{a2} and θ_{a3} correspond to the first, second, third, and fourth resonant frequencies, respectively. Moreover, f_0 through f_3 represent the first through fourth resonance frequencies, respectively [46-48].

$$\theta_{a0} = 2\tan^{-1}\left(\frac{1}{\pi f_0 Z_t \left(C_D + C_g \right)} \right)$$

$$\theta_{a1} = 2\pi - 2\tan^{-1}\left(\pi f_1 Z_t \left(C_D + C_g \right) \right)$$

$$\theta_{a2} = 2\tan^{-1}\left(\frac{1}{\pi f_2 Z_t \left(C_D + C_g \right)} \right)$$

$$\theta_{a3} = 2\pi - 2\tan^{-1}\left(\pi f_3 Z_t \left(C_D + C_g \right) \right) \quad (3)$$

From (3), it is clear that the capacitance C_D and C_g have an effect on all resonance frequencies, with the largest impact on the second and fourth resonant frequencies. This allows the capacitance value to be utilized to regulate the resonant frequency by raising or reducing it. As a result, the phase value on the S-curve may be controlled according to the frequency range at an angle of 0-90 degrees, which is the phase angle used to reflect the waves of the antenna. The antenna's radiation pattern with the EBG reflector is directional. Table I provides a summary of the parameters of the EBG unit cell depicted in Fig. 3.

According to the design of the aforementioned unit cell, the capacitance may control the first, second, third, and fourth resonance frequencies. Fig. 4 depicts the capacitance between connected unit cells when the unit cell array is used as an antenna reflector. The resultant capacitance is denoted by C_a. Moreover, the region between pins, which are the two unit cells and the ground plane, generates the inductive L_p, as seen in Fig. 5. Based on the aforementioned findings, it was determined that the resultant C_a value influences the bandwidth coverage of the resonant frequency range at the 0 - 90 degree phase angle but has a negligible effect on the

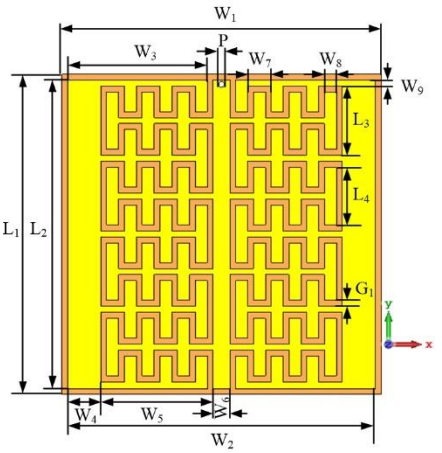

FIGURE 3. The configuration and parameters of the EBG unit cell structure.

TABLE I
PARAMETERS OF THE EBG UNIT CELL

Parameters of EBG unit cell	
W_1 = 12.00 mm.	W_9 = 1.27 mm.
W_2 = 11.58 mm.	L_1 = 12.00 mm.
W_3 = 5.25 mm.	L_2 = 11.58 mm.
W_4 = 1.27 mm.	L_3 = 2.61 mm.
W_5 = 4.02 mm.	L_4 = 2.51 mm.
W_6 = 0.63 mm.	G_1 = 0.32 mm.
W_7 = 0.89 mm.	h = 0.79 mm.
W_8 = 0.45 mm.	P = 0.22 mm.

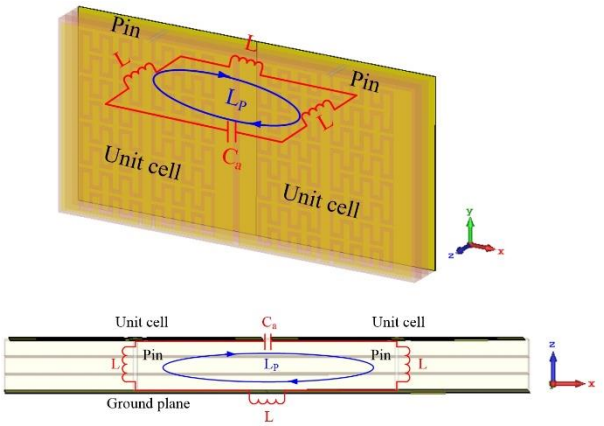

FIGURE 4. The effects of connectivity between the unit cell structure.

required resonance frequency range. Thus, an appropriate value of C_a must be determined such that the resonance frequency band remains unchanged and the requisite bandwidth coverage is attained. The simulation results will be presented in the next section. In establishing the resonant

frequency range, it is necessary to combine the C_a value with (3), which may be written as (4).

$$\theta_{a0} = 2\tan^{-1}\left(\frac{1}{\pi f_0 Z_t\left(C_D + C_g + C_a\right)}\right)$$

$$\theta_{a1} = 2\pi - 2\tan^{-1}\left(\pi f_1 Z_t\left(C_D + C_g + C_a\right)\right)$$

$$\theta_{a2} = 2\tan^{-1}\left(\frac{1}{\pi f_2 Z_t\left(C_D + C_g + C_a\right)}\right)$$

$$\theta_{a3} = 2\pi - 2\tan^{-1}\left(\pi f_3 Z_t\left(C_D + C_g + C_a\right)\right) \quad (4)$$

When

$$C_a = \frac{W\varepsilon_0(1+\varepsilon_r)}{\pi}\cosh^{-1}\left(\frac{a}{g}\right),\ L_p = \mu_0\mu_r h$$

From Equation (4), it is evident that the C_a value created during the unit cell connection must be incorporated into the capacitance value provided by the unit cell structure. Consequently, it is possible to explain why the C_a values in conjunction with the capacitive values of the unit cell structure, i.e. C_D and C_g, have an influence on the overall resonant frequency. When a is the range of unit cell and width gap being the gap width g The simulation results based on the unit cell design provided in this part are shown in the next section.

III. THE SIMULATION OF EBG

In this part, the structure of the EBG unit cell developed in the previous section will be simulated to evaluate the efficiency of the unit cell structure. It is separated into two sections: The first section consists of the simulation results for the structure of a single unit cell and for arranging the array of unit cells to be utilized as the antenna's reflector. The second section is to simulate the operation when a reflector formed from an EBG unit cell array is coupled to a dipole antenna at each of the reflector's resonant frequencies to verify the resonance and gain characteristics of the antenna.

A. THE SIMULATION OF SINGLE EBG UNIT CELL TO ARRAY EBG UNIT CELL

In this section, the EBG unit cell structure has simulated the properties by establishing the Boundary condition of the Perfect electric conductor (PEC) and the Perfect Magnetic Conductor (PMC) alternately along the *X* and *Y*-axes. the *Z*-axis is set as the direction of the incident wave with a frequency of 1-7 GHz on the unit cell to evaluate the frequency response, as indicated in Fig. 6. The dimensions of the unit cell structure are provided in Table I. To calculate the response of the electric field for the antenna arrangement based on the direction of the current, the wave propagation of the antenna

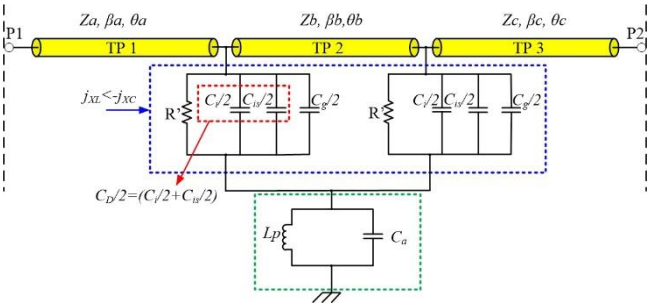

FIGURE 5. The equivalent circuit of connect unit cell.

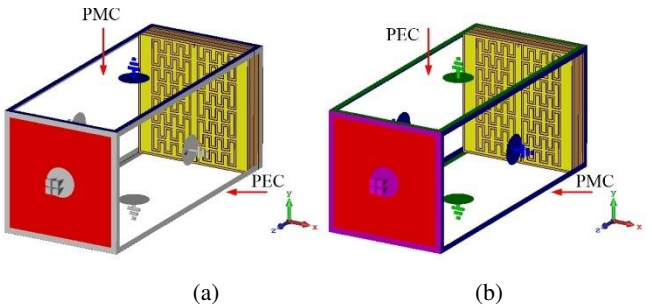

FIGURE 6. The simulation configurations of the unit cell with (a) E- field in the *X*-polarization and (b) E- field in the *Y*-polarization.

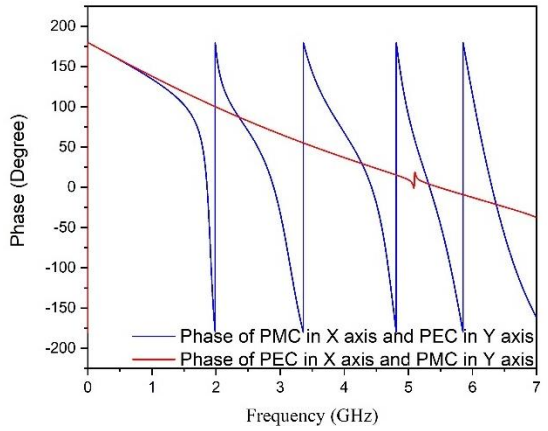

FIGURE 7. The simulation results of phase angle on the unit cell with setting PMC and PEC in the *X*-polarization and *Y*-polarization.

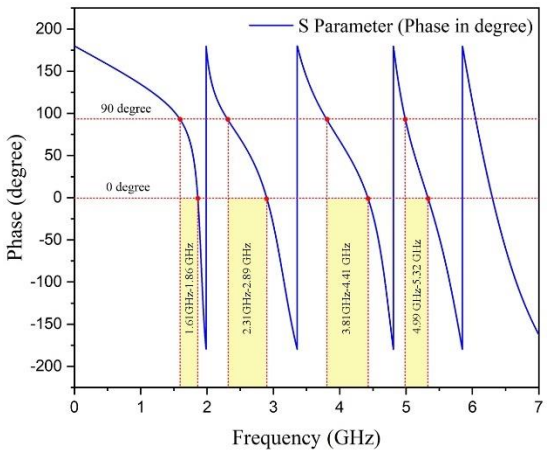

FIGURE 8. The simulation results of the phase angle on unit cell with setting PEC in the y-polarization.

must correspond with the electric field's direction. Fig. 6(a) displays PEC on the *X*-axis and PMC on the *Y*-axis. Fig. 6(b) displays PMC on the *X*-axis and PEC on the *Y*-axis. The port spacing in both configurations is $\lambda/2$ of the fundamental frequency of 1.8 GHz. The simulation results depicted in Fig. 7 indicate that assigning the *X*-axis to PMC and the *Y*-axis to PEC causes the phase shift in the resonant frequency range to be characterized by an S-curve corresponding to the desired frequency range, allowing the frequency band to cover the bandwidth in the resonant frequency range at an angle of 0-90 degrees to be utilized as a reflector combination with an antenna propagating along the *Z*-axis. By arranging the PEC along the *Y*-axis, which corresponds to the direction of the antenna's current flow. It is discovered that the frequency response can cover the resonant frequency ranges of 1.8 GHz (1.61 GHz-1.86 GHz), 2.45 GHz (2.31 GHz-2.89 GHz), 4.3 GHz (3.81 GHz-4.41 GHz), and 5.2 GHz (4.99 GHz-5.32 GHz), which correspond to the frequency ranges of LTE, WLAN, and Altimeter, as shown in Fig. 8. In the case of setting the PEC on the *X*-axis and the PMC on the *Y*-axis as shown in Fig. 7, the phase shift is not detected in the specified resonant frequency range, indicating that the structure of the double interdigital unit cell has the response for PEC along only the *Y*-axis, which is in the same direction as the antenna's current flow. As evident in the numerical simulation section, the proposed structure is essentially linearly polarized. This presents a significant limitation, given that several multi-band AMC metasurfaces [33-36] have already been presented in the literature, capable of responding independently to wave polarization. However, the designed structure exhibits the behavior of the unit cell as a one-dimensional electromagnetic band gap structure.

In addition to the ICPW [26], [27], [40], [41] infrastructure that enhances the capacitance between the transmission line and the semi-ground to control the resonant frequency, it was discovered that the capacitive value of the double interdigital range, that is C_D value, can substantially increase the capacitive value on the unit cell structure for controlling resonance in the desired frequency range. These values are dependent on the number of fingers, the finger's width, and its length. Fig. 9 depicts the simulation result when the number of fingers is altered. It has been determined that increasing the number of fingers affects the phase in the resonance frequency band. The unit cell structure is ICPW if the number of fingers is zero. However, if we increase the number of fingers to two and three, the phase of the resonant frequency will move closer to zero. This implies that increasing the number of fingers will provide more capacitance than the ICPW structure, consequently enhancing the slow wave on the transmission line. This permits the proposed structure to respond to multiple frequencies and is considerably smaller than the conventional $\lambda/8$. Fig. 10 depicts a simulation result for adjusting the parameter W_8 of finger width. It has been discovered that the phase shift at the first resonant frequency is slightly altered, whereas the phase shift at higher frequencies is significantly

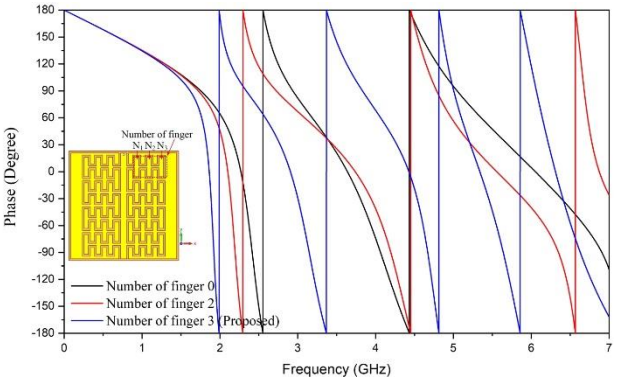

FIGURE 9. The simulation results of the phase angle on the proposed unit cell as adjusting the finger number.

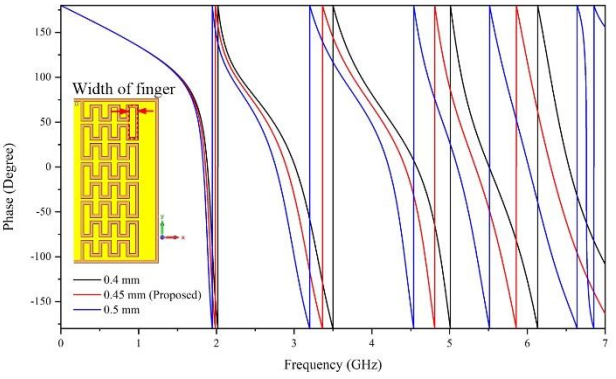

FIGURE 10. The simulation results of the phase angle on the proposed unit cell as adjusting the finger width (W_8).

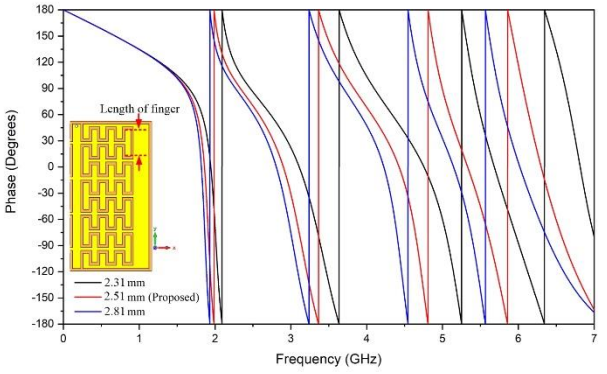

FIGURE 11. The simulation results of the phase angle on the proposed unit cell as adjusting the finger length (L_4).

impacted. Then, the parameter L_4 of the finger length will be investigated as depicted in Fig. 11. It is indicated that phase shifts at the first resonant frequencies are minimally impacted, while phase shifts at higher frequencies will be greatly affected when a finger length is appropriate. It is explained that increasing or decreasing the capacitive value in the double interdigital region with the width or length of the finger has a negligible effect on the phase shift at the first resonant frequency, but a substantial effect at higher frequencies. This indicates that the capacitive value and slow wave effect of the unit cell structure have increased drastically.

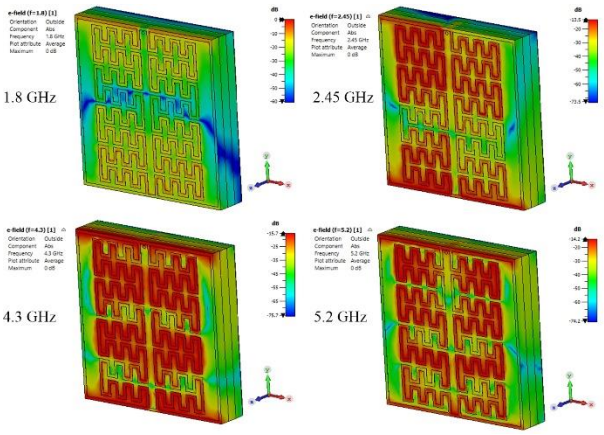

FIGURE 12. **The simulation result of E- field on the Y-axis and H- field on the *X*-axis.**

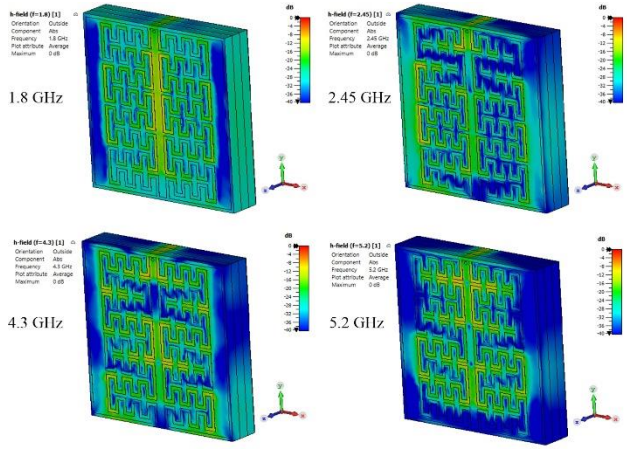

FIGURE 13. **The simulation result of E- field on the *X*-axis and H- field on the *Y*-axis.**

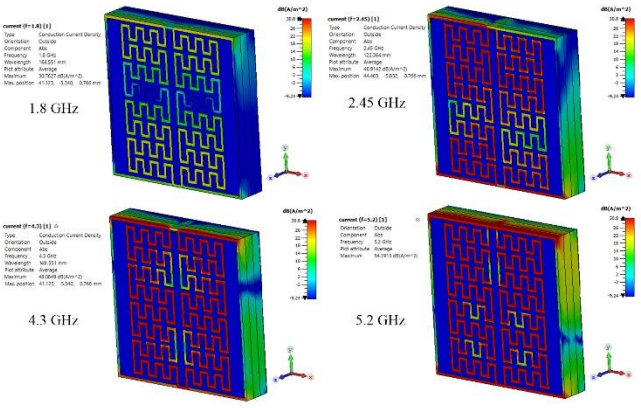

FIGURE 14. **The simulation result of current distribution on the surface of proposed unit cell.**

Fig. 12 depicts the simulation result of the Electromagnetic field effect caused by exciting the electric field on the structure of the unit cell when the electric field and magnetic field directions were set along the *Y*-axis and the *X*-axis, respectively. It is discovered that the electric field has a significant impact on the double interdigital region at all resonant frequencies. As illustrated in Fig. 13, when the

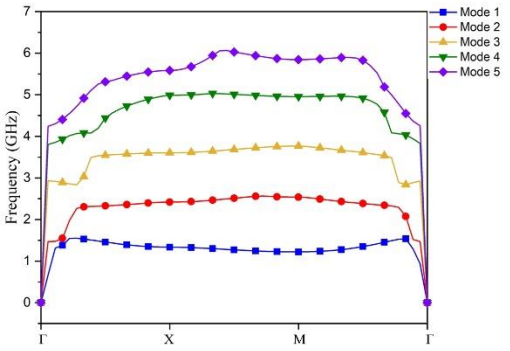

FIGURE 15. **The dispersion diagram of proposed unit cell.**

electric field is along the *X*-axis and the magnetic field is along the *Y*-axis, the effect of the electric field in the double interdigital region is minimal. The simulation to evaluate the current density on the surface of the unit cell structure, as depicted in Fig. 14, revealed that at all resonant frequencies, there were very strong currents in the double interdigital gap region, but there is no current density on the surface of the unit cell structure. Particularly at high frequencies, it is demonstrated that the double interdigital gap region has a capacitance value so high that it can be used to control the resonant frequency. According to the simulation results of the electric field and current density effects, the capacitive value in the double-digit region of the unit cell has a satisfactory response along the PEC direction along the *Y*- axis. In order to reflect more efficiently than a conventional reflector when the unit cell is arranged in an array, it is recognized that the antenna's *Y*-axis flow direction must be aligned with the positioning direction of the proposed unit cell.

Fig. 15 demonstrates the simulation result of the dispersion diagram [19], [23-26], which represents the free surface wave range of the EBG unit cell by using CST eigenmode solver. It has been found that the free surface wave range is between 1.66 GHz – 2.3GHz, 2.2 GHz -3.6 GHz, 3.6 GHz- 4.8 GHz, and 4.8 GHz - 5.59 GHz, encompassing the frequency range with an S-curve phase as shown in Fig.8. As the results, it is possible to explain why there are no surface waves in the resonant frequency range of the proposed EBG unit cell structure, and only wave propagation that causes resonance in that frequency range. Based on the results of previous simulations,

Comparing the simulation results of EBG unit cell structures created with the same type of printed circuit board using the double interdigital technique with $\lambda/8$ and the typical EBG unit cell structures with $\lambda/2$ is depicted in Fig. 16. It has been determined that the phase response at the first resonant frequency of the double interdigital technique $\lambda/8$ is less than that of the typical technique with $\lambda/2$. Consequently, the two EBG unit cell configurations at the same fundamental frequency of 1.8 GHz have a substantial structural difference, resulting in the EBG unit cell using the double interdigital technique being significantly smaller. Additionally, it can control the phase shift of second to fourth-order resonant

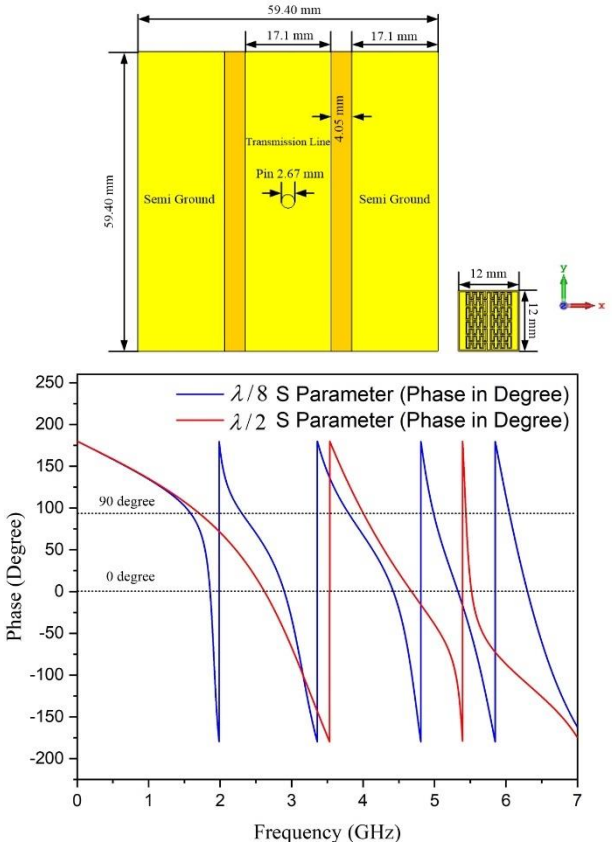

FIGURE 16. **The comparison results of the S-parameter's phase angle between proposed technique (λ//8) and typical technique (λ//2).The simulation result of current distribution on the surface of proposed unit cell.**

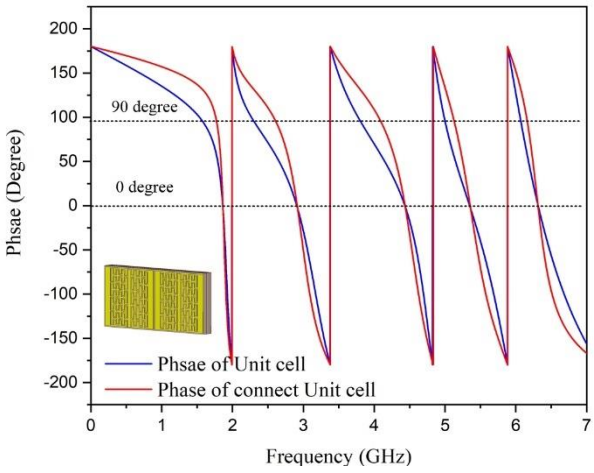

FIGURE 17. **The comparison results of the S-parameter's phase angle between single unit cell and connected unit cell.**

frequencies within the required frequency range. The conventional EBG unit cell structure cannot manipulate the resonance frequency as effectively as the proposed technique.

While EBG unit cells are connected as depicted in Figs. 4 and 5, a capacitive value of C_a can be observed between the unit cells. Fig. 17 illustrates a comparison between the phase results of a solitary unit cell and a connected unit cell. It is

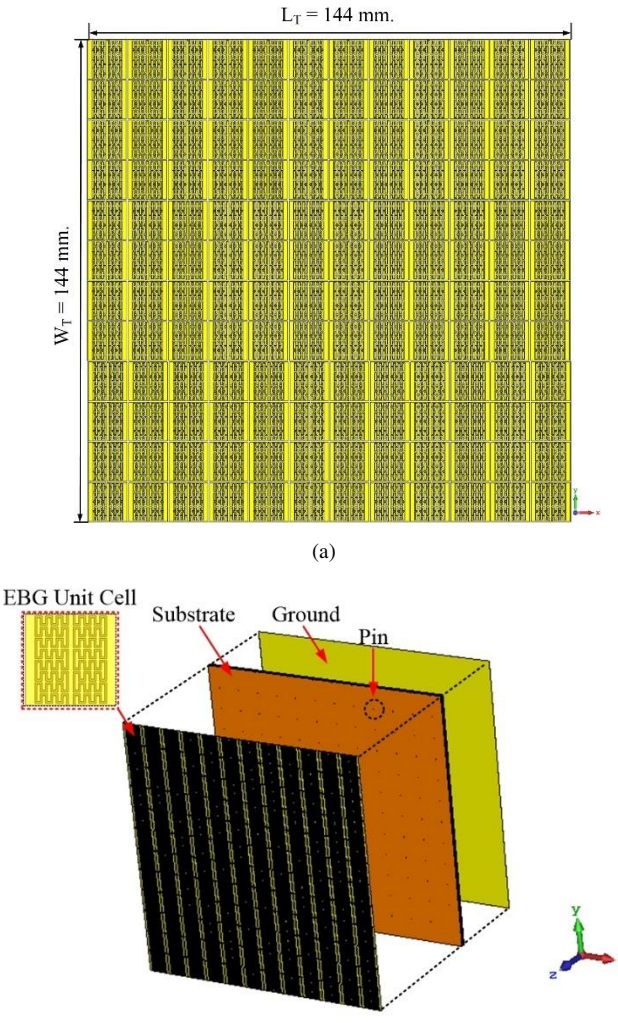

FIGURE 18. **The reflector configurations of array EBG unit cell with 12x12 with (a) two-dimension (b) three-dimension.**

clearly found that the resonant frequency does not change. In addition, using the value of C_a to simulate the experiment revealed that there is no phase result alteration within the resonant frequency range. However, it will affect the slope of the S-curve in the range of 0-90 degrees encompassing the resonant frequency range and will have a negligible impact on the simulation results. As a consequence, the C_a value has a negligible effect on the phase shift across the resonant frequency range and can accommodate the desired frequency range. Thus, a large number of EBG unit cells can be connected together to create an antenna reflector without influencing the phase shift. Therefore, the EBG unit cell is arranged in an array of 12×12 unit cells with an overall dimension of 144 mm ×144 mm, which is adequate for covering the size of the dipole antenna to be used in all frequency ranges, as depicted in Fig. 18. The next section will present the simulation results of the array EBG unit cell used as a reflector in conjunction with the antenna.

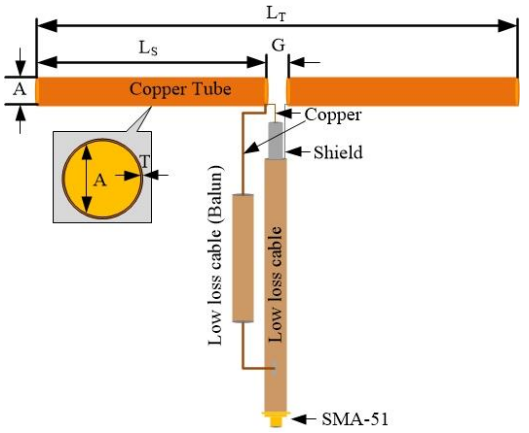

FIGURE 19. **The dipole antenna configuration created by copper tube connected to balun and fed by SMA-51.**

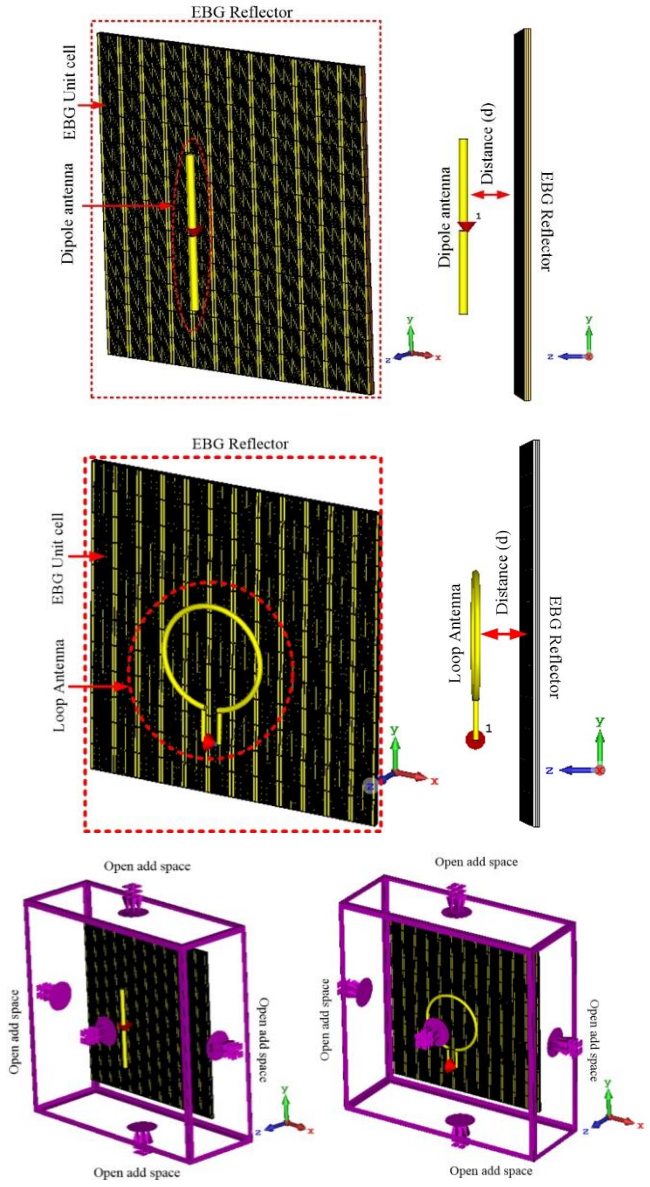

FIGURE 20. **The configuration of the proposed array EBG unit cell with the designed dipole/loop and the boundary condition setting of the antenna with the proposed EBG reflector.**

TABLE II
DIPOLE ANTENNA DIMENSION

Dipole parameters	Dimension (mm)			
	f = 1.8 GHz	f = 2.45 GHz	f = 4.3 GHz	f = 5.2 GHz
L_S	32.50	22.25	12.50	10.5
L_T	68.00	47.0	26.50	22.0
G	3.00	2.5	1.50	1.00
A	3.46	3.46	3.46	3.46
T	0.46	0.46	0.46	0.46

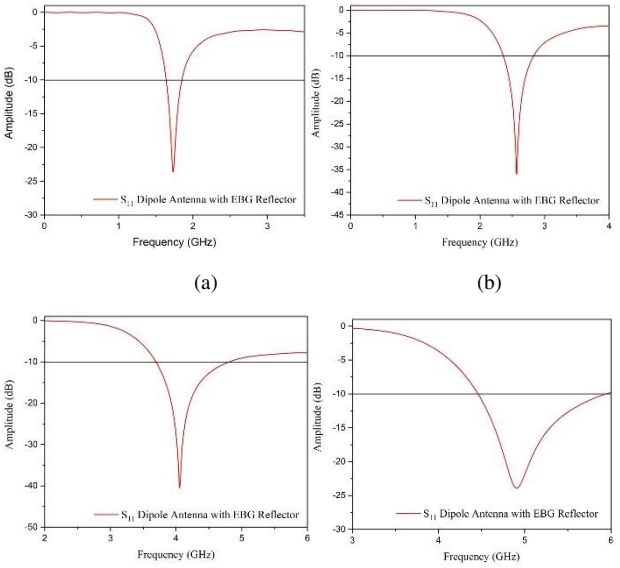

FIGURE 21. **The simulated return losses of the proposed EBG reflector with a dipole antenna at (a) 1.8 GHz, (b) 2.45 GHz, (c) 4.3 GHz, and (d) 5.2 GHz**

B. THE SIMULATION OF REFLECTOR FORMED BY ARRAY EBG UNIT CELL CONNECTED WITH A DIPOLE ANTENNA AND LOOP ANTENNA

This section discusses the simulation findings of attaching a dipole antenna as an electric source and a loop antenna as a magnetic source to an EBG reflector designed in the previous section. The reflector will be equipped with either a dipole antenna or a loop antenna, designed to respond to a single frequency at the same frequency as the EBG reflector: 1.8 GHz, 2.45 GHz, 4.3 GHz, and 5.2 GHz. The antenna consists of a copper conduit connected to a low-loss RG-42 cable and a balun. Fig. 19 depicts the proposed dipole antenna structure fed by SMA-51, and Table II lists the parameters of each antenna at its resonance frequency. The dipole antenna exhibits an omnidirectional radiation pattern, while the loop antenna's radiation pattern is bidirectional. The dipole antenna gains are 2.82 dBi, 2.53 dBi, 2.42 dBi, and 2.31 dBi, while the loop antenna gains are 3.31 dBi, 3.49 dBi, 3.1 dBi, and 3.33

This article has been accepted for publication in IEEE Access. This is the author's version which has not been fully edited and content may change prior to final publication. Citation information: DOI 10.1109/ACCESS.2024.3369477

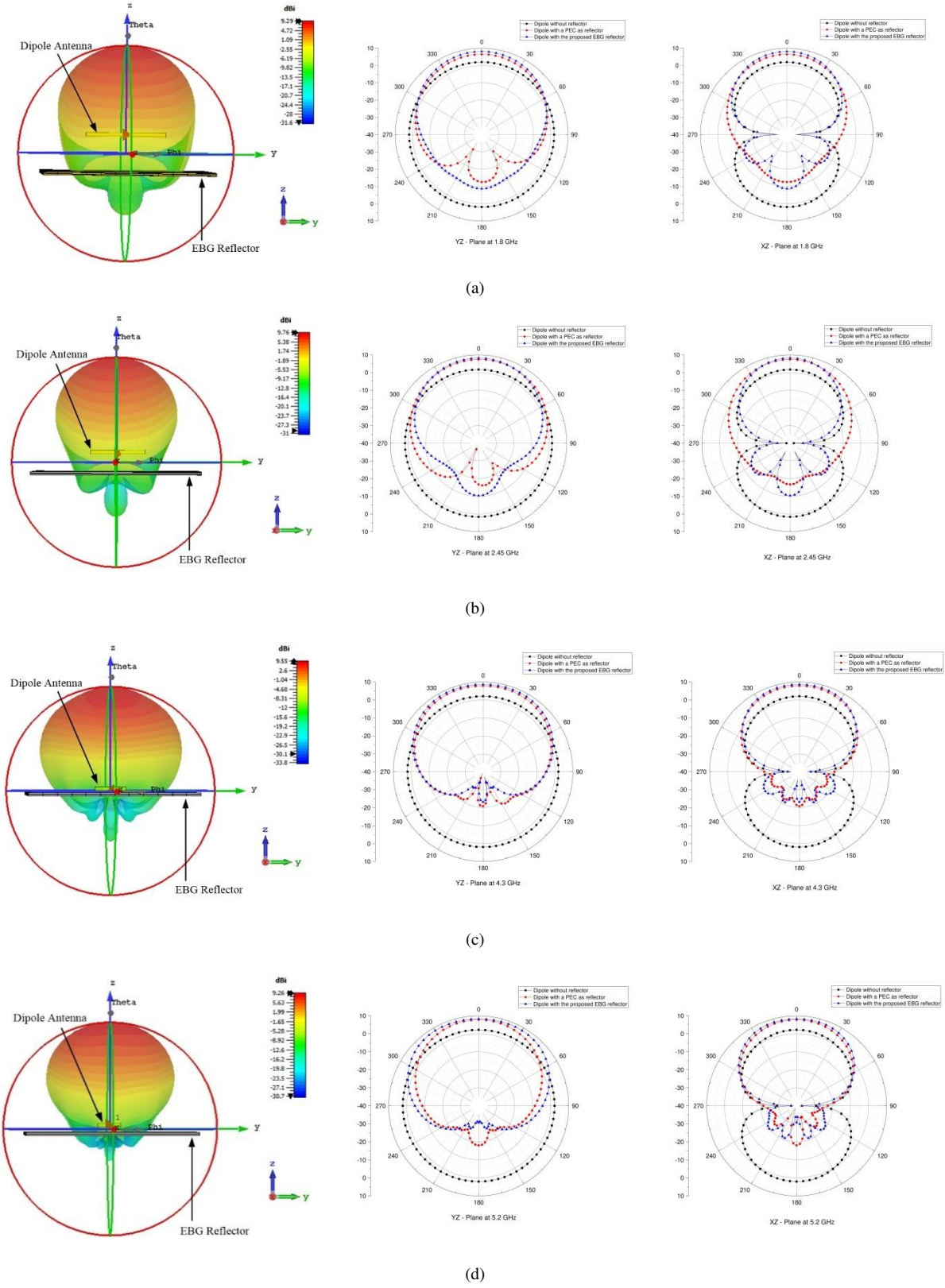

FIGURE 22. **The simulated radiation pattern of a dipole antenna with and without the proposed EBG reflector at (a) 1.8 GHz, (b) 2.45 GHz, (c) 4.3 GHz, and (d) 5.2 GHz.**

This article has been accepted for publication in IEEE Access. This is the author's version which has not been fully edited and content may change prior to final publication. Citation information: DOI 10.1109/ACCESS.2024.3369477

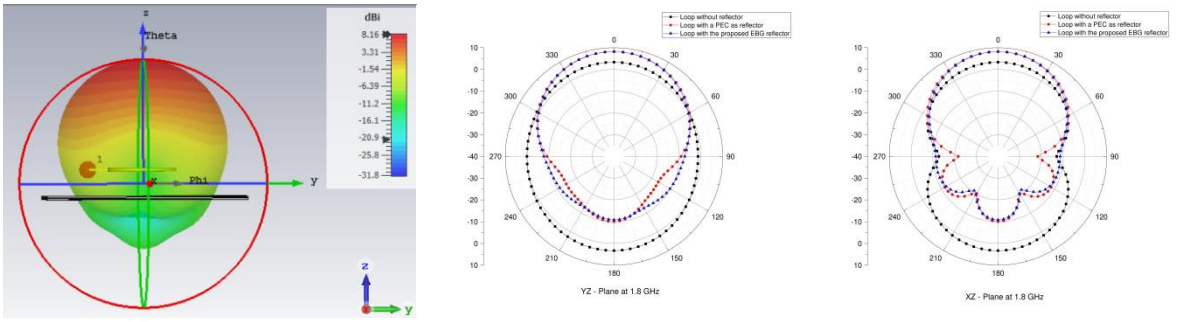

(a)

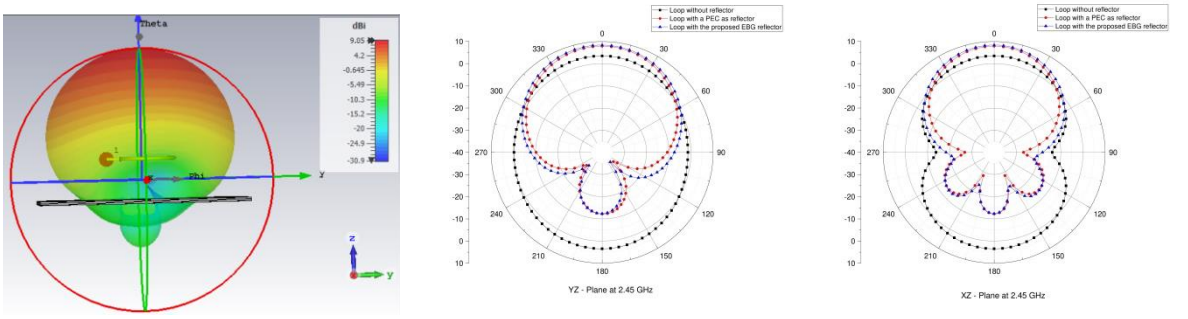

(b)

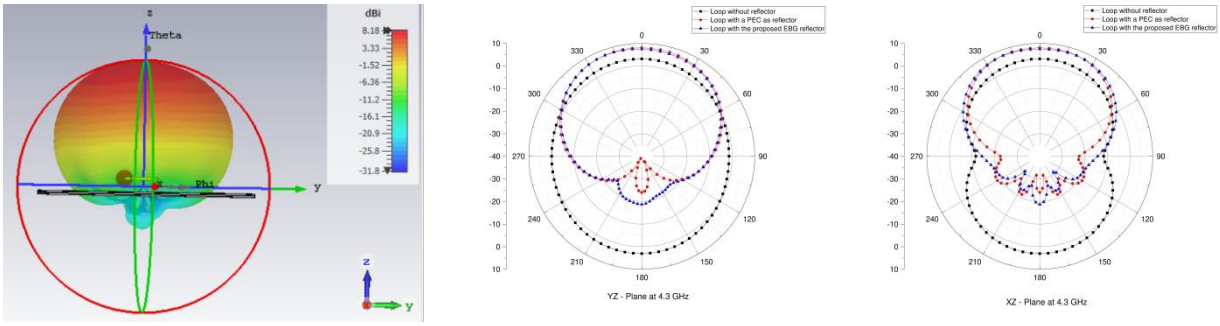

(c)

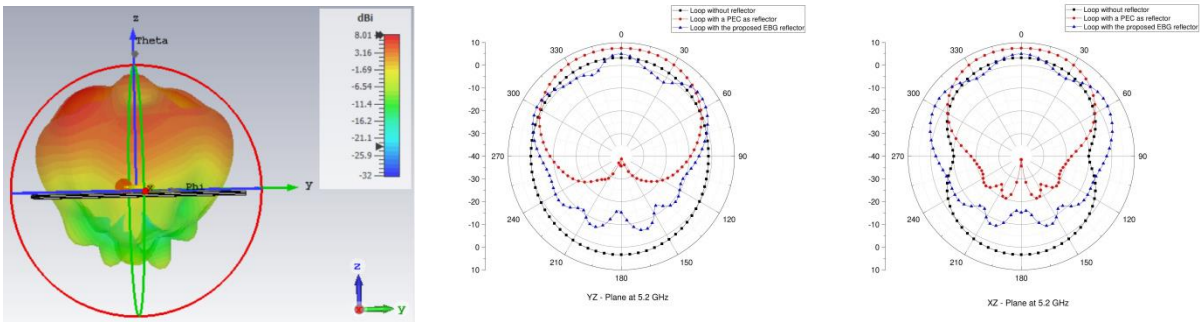

(d)

FIGURE 23. The simulated radiation pattern of a loop antenna with and without the proposed EBG reflector at (a) 1.8 GHz, (b) 2.45 GHz, (c) 4.3 GHz, and (d) 5.2 GHz.

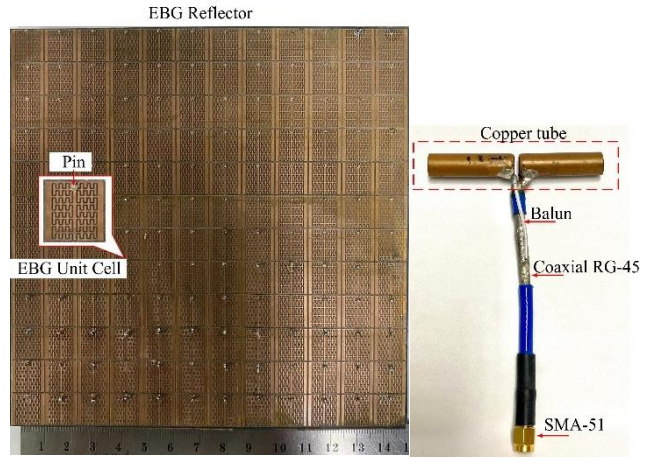

(a)

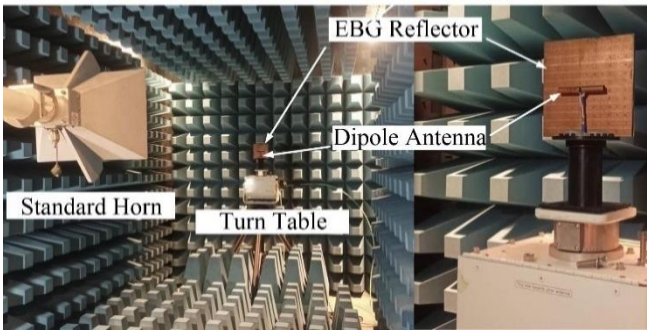

(b)

FIGURE 24. **(a) The fabricated EBG reflector and the dipole antenna and (b) the measurement setup for the antenna in chamber room.**

dBi at 1.8 GHz, 2.45 GHz, 4.3 GHz, and 5.2 GHz, respectively, with impedance matching below -10 dB at all resonant frequencies. The dipole/loop antenna was then linked to the EBG reflector by placing it at a distance of *d* in front of the reflector. The antenna is aligned along the *Y*- axis, which corresponds to the simulation of an EBG unit cell with PEC arranged along the *Y*-axis. Considering the distance '*d*' from Fig. 8, the phase of the electromagnetic wave reflected on the EBG is shifted by an angle β ranging between −90° and +90° relative to the incident electromagnetic wave. This phenomenon occurs only for specific frequencies. Additionally, we positioned the dipole source near the EBG reflector, resulting in an in-phase reflected wave and avoiding mutual coupling between the dipole source and the reflector. At resonance frequencies of 1.80 GHz, 2.45 GHz, 4.3GHz, and 5.2 GHz, the distance between the antenna and the EBG reflector (d) is 39.09 mm, 22.4 mm, 11.54 mm, and 8.23 mm, respectively. Fig. 20 depicts the configuration of array EBG unit cell boundary conditions by assigning Open add space to the *X*, *Y*, and *Z*-axis planes. Fig. 21 shows the simulation return loss of the proposed reflector with a dipole antenna. It has been found that the resonant frequency with impedance matching below -10 dB is about at 1.8 GHz with a bandwidth of 190 MHz (1.66 GHz -1.85 GHz), 2.45 GHz with a bandwidth of

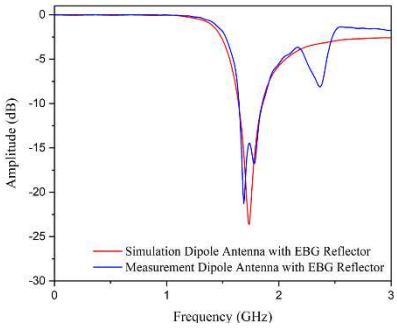

(a)

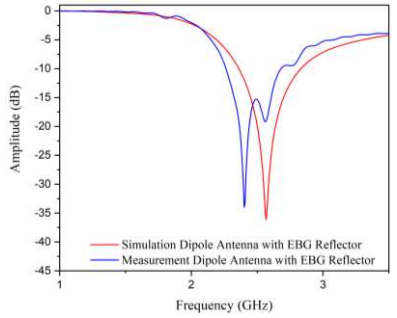

(b)

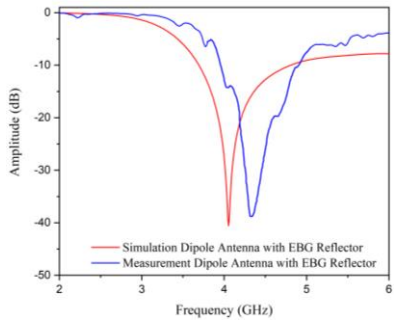

(c)

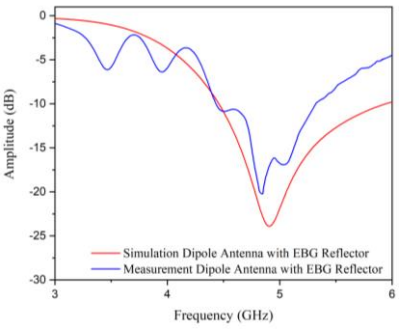

(d)

FIGURE 25. **The comparison of simulated and measured return losses of the dipole antenna with EBG reflector at (a) 1.8 GHz, (b) 2.45, (c) 4.3 GHz, and (d) 5.2 GHz.**

480 MHz (2.35 GHz -2.83 GHz), 4.3 GHz with a bandwidth of 1.11 GHz (3.63 GHz -4.74GHz), and 5.2 GHz with 1.39 GHz (4.53 GHz -5.92 GHz) as shown in Figs. 21 (a) to (d),

respectively. Figs. 22 and 23 (a) to (d) illustrate the antenna's radiation patterns with peak gain. The dipole antenna with the proposed EBG reflector gains at resonance frequencies of 1.80 GHz, 2.45 GHz, 4.3 GHz, and 5.2 GHz are approximately 9.29 dBi, 9.76 dBi, 9.55 dBi, and 9.26 dBi, respectively. Furthermore, the radiation pattern at each resonant frequency is directional, resulting in an improved gain of approximately 7 dBi for dipoles and 5.5 dBi for loops, respectively. When compared with a dipole with a PEC as a reflector, it can improve the gain by 1-2 dBi due to the prevention of surface waves. According to the results of the simulation, the antenna gain has significantly enhanced at all resonant frequencies. This demonstrates that the proposed EBG reflector prevents surface waves and has wave propagation that significantly improves the antenna phase, resulting in the proposed reflector exhibiting greater antenna gain than a conventional reflector. Next, the dipole antenna with the proposed EBG reflector will be fabricated and the results will be evaluated in the subsequent section.

IV. MEASUREMENT RESULTS

This section describes the fabrication and evaluation of the antenna with the proposed EBG reflector. It will be manufactured on an RT duroid 5880 printed circuit board with epsilon (ε_r) 2.2, a thickness of 0.79 mm, and a loss tangent ($\tan\delta$) of 0.0004. The reflector's dimensions are 144 mm ×144 mm, and it was created using a milling machine. In addition, each of the four single-frequency dipole antennas connected to the reflector is constructed with a copper tube and a low-loss RG-45 cable. Utilizing a balun circuit, the balance line is created. The SMA-51 connector is utilized in the feed section. Fig. 24(a) depicts the structure of the dipole antenna and the proposed reflector.

Each frequency dipole used to test the EBG reflector operates at its fundamental frequency, exhibiting coherent radiation that resonates with the electron beam. The properties of the antenna with reflector are evaluated in a chamber room, as depicted in Fig. 24(b), where the designed dipole antenna was positioned in front of the EBG reflector at the distance corresponding to the simulation. Fig. 25 depicts a comparison between the simulation and measurement results of the dipole antenna with the proposed EBG reflector. The result demonstrates that the antenna's return loss (S_{11}) is less than -10 dB at all frequencies examined. The bandwidth range for the 1.8 GHz frequency is 170 MHz (1.69 GHz – 1.86 GHz), whereas the bandwidth range for the 2.45 GHz frequency is 360 MHz (2.28 GHz – 2.64 GHz). At 4.3 GHz, it has a bandwidth of 560 MHz (4.15 GHz – 4.71 GHz) and the bandwidth is 910 MHz (4.45 GHz – 5.36 GHz) at 5.2 GHz. There will be a change in impedance matching in the 2.45 GHz and 4.3 GHz bands, but the operating frequency range will remain unaffected. According to the experimental findings, there is a strong correlation between the simulated and actual measurement outcomes.

Figs. 26 and 27 show the testing of the radiation pattern in *XZ* and *YZ*-planes, respectively. It is revealed that all resonance frequencies had directional propagation, with strong propagation in the co-polarization at *XZ* and *YZ*-planes and weak propagation in the cross-polarization at *XZ* and *YZ*-planes. The measured antenna gain at 1.8 GHz, 2.45 GHz, 4.3 GHz, and 5.2 GHz is approximately 8.29 dBi, 8.76 dBi, 8.55 dBi, and 8.22 dBi, respectively. Evidently, the measurement findings closely resemble the simulated findings, and it can be concluded that the designed EBG reflector can substantially increase the antenna's gain in the desired resonant frequency range.

V. CONCLUSION

The design of a multiband EBG reflector using the double interdigital technique on a unit cell is presented. The double interdigital technique was developed based on CPW collaboration with the interdigital technique to increase the capacitance on the transmission line end of the unit cell compared to the ICPW technique. Consequently, an increase in the capacitance of a unit cell causes the occurrence of a very slow wave on the transmission line. Resultantly, the electrical length and physical length of the transmission line are not equal. As a result, the physical structure dimension of the proposed unit cell can be dramatically reduced compared to the typical unit cell structure size. It has been determined that the dimensions of the proposed unit cell decrease from λ/2 to λ/8 at the resonant frequency of 1.8 GHz. The proposed unit cell size is about 12 mm × 12 mm. Additionally, the resonance frequency can be controlled to achieve the desired resonance frequency by increasing or decreasing the capacitive value in the double interdigital region. This capacitive effect applies to the shifts of all resonance frequencies away from the first resonant frequency and has a substantial effect on the shifts of the second and fourth resonant frequencies. Based on this technique, it is possible to design a small EBG unit cell with multiple frequency responses. When the EBG unit cell is arranged in a 12 × 12 array to serve as a multi-band EBG reflector, the proposed reflector has overall dimensions of 144 mm × 144 mm. Then, the proposed reflector is positioned in front of a single-frequency dipole antenna; the simulated results indicate the impedance matching below -10 dB across all resonant frequencies and the antenna gains of 9.29 dBi, 9.76 dBi, 9.55 dBi, and 9.26 dBi, respectively, at 1.8 GHz (LTE), 2.45 GHz (WiFi), 4.3 GHz (Altimeter), and 5.2 GHz (WiFi). During measurements and evaluation of the EBG reflector in the chamber, it was determined that the antenna had an impedance matching of less than -10 dB. All resonant frequencies can cover within the desired frequency band, which may have been altered slightly from the simulated results but remained within the specified frequency range. Moreover, the measured radiation patterns of a single-frequency dipole antenna with the proposed EBG reflector. maintain a directional pattern in the *XZ*-plane and *YZ*-plane at each resonant frequency. At the resonant frequency of 1.8

GHz, 2.45 GHz, 4.3 GHz, and 5.2 GHz, the antenna gains are 8.29 dBi, 8.76 dBi, 8.55 dBi, and 8.22 dBi, respectively.

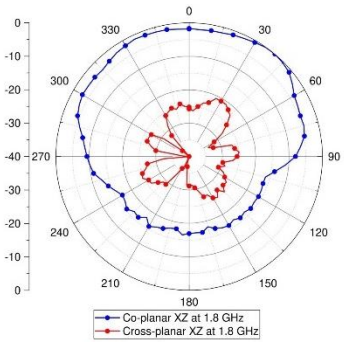

(a)

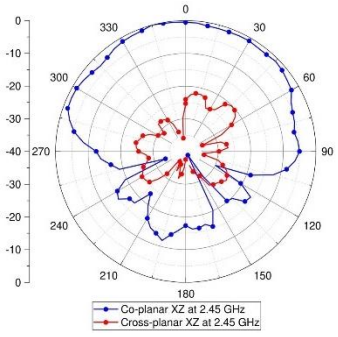

(b)

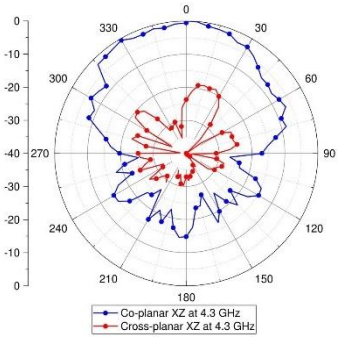

(c)

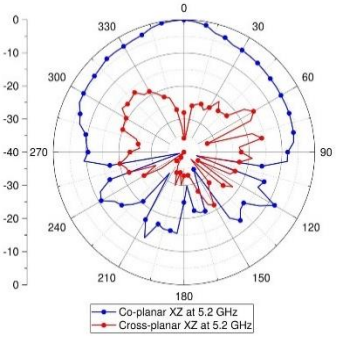

(d)

FIGURE 26. Measured results of *XZ*-Planes radiation patterns at (a) 1.8 GHz, (b) 2.45 GHz, (c) 4.3 GHz, and (d) 5.2 GHz.

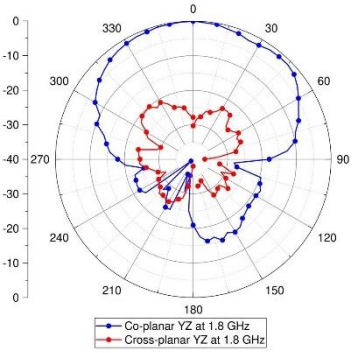

(a)

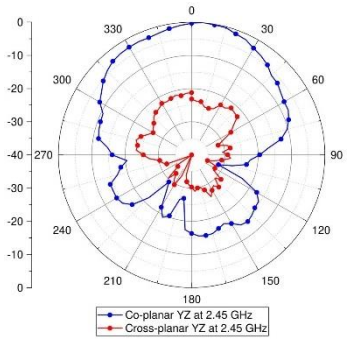

(b)

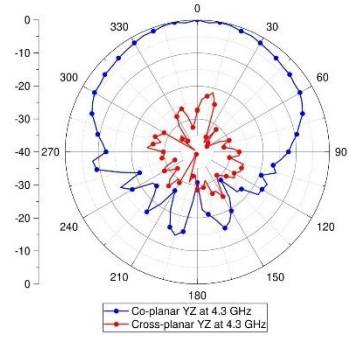

(c)

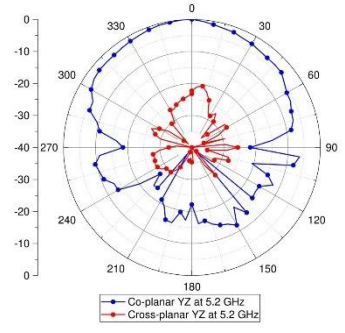

(d)

FIGURE 27. **Measured results of *YZ*-Planes radiation patterns at (a) 1.8 GHz, (b) 2.45 GHz, (c) 4.3 GHz, and (d) 5.2 GHz.**

TABLE III
UNITS FOR MAGNETIC PROPERTIES COMPARISON OF THE PROPOSED EBG REFLECTOR WITH ANTENNA IN REFERENCES

Reference Number	No. of bands (structure shaped)	Freq.(GHz)	Unit cell size (mm^3)	Overall size (mm^3)	No. of unit cell array	Measurement gain (dB)	Efficiency	Type of Applications
[17]	1 (Fork like EBG)	2.46	15.5 ×8×0.78	15.5×38	4(Tx)×4(Rx)	-	92.11107%	EBG duplexer
[18]	2 (IE-EBG spiral)	1.2-2 , 3.42-3.5	10×10×2.2	100×100×2.2	10×10	-	-	EBG for Multichip
[19]	2 (Square patch PBG)	6.3-9.65 9.3-11.6	7×7×1.5	365×365×1.5	50×50	-	-	EBG for suppression
[20]	5 (DAU-EBG)	2.3-2.6, 4.1-5, 5.9-6 (X direction) 2.5-2.9, 4.8-6 (Y direction)	8.6×8.6×2	51.6×51.6×2	6×6	-	-	Multiband EBG
[21]	3 (Meander line EBG)	2.4, 3.6 and 5.2	7×7×1.57	77×49	11×7	3.5, 4.2 and 6.19	93.6282%, 91.007% and 91.58%	EBG Reflector
[22]	5 (2 layer Circular)	2.45,3.6 with 1.8, 3.83, 5.5	Radius 4 and 3	8×6×1.6	2×1 and 2×1	-	-	Multiband EBG
[24]	3 (Square patch)	2.45 5.34 9.35	3×3×1.6	14×3×1.6	4	-2,3 and 2	98.672%,96.775% and 92.978%	Operating multi-band antenna
[25]	1 (Square corner-truncated)	5.5	11.5×11.5×2.5	92×92×2.5	8×8	8.25	95.98%	EBG gain enhancement
[26]	3 (ICPW)	1.8 2.45 3.7	18×18×3.2	181×181×1	10×10	8.72 8.16 8.10	97.96%,98.13% and 98.90%	EBG Reflector
[27]	2 (Split ring open loop)	1.8, 2.6	12×12×1.6	13×9×1.6	300×200×1.6	-	-	EBG control main beam
[40]	1 (Square patch with Square slot)	12.4	6×6×1.6	42×42×1.6	7×7	-	-	EBG Reflector for cavity
EBG proposed	4 (Interdigital)	1.8, 2.45, 4.3, 5.2	12×12×2.37	144×144×2.37	12×12	8.29 8.76 8.55 8.22	97.46%,98.76%,98.65% and 98.07%	Multi band Reflector

However, the co-polarization and cross-polarization have very different intensities because the antenna with the proposed reflector is linearly polarized. According to the simulated and measured results, they are nearly similar. In conclusion, the proposed reflector can improve the antenna's gain efficiency and perform in multiple frequency bands. Furthermore, the unit cell dimension of the proposed EBG reflector is much smaller than that of the reference reflector presented in Table III. Therefore, it is suitable for use in a variety of applications, including as a reflector for enhancing antenna gain in base stations, radar systems, GPR systems, and satellite systems.

ACKNOWLEDGMENT

This work was supported by King Mongkut's University of Technology North Bangkok contract no. KMUTNB-65-know-31, and in part by the Engineering and Physical Science Research Council under Grant EP/S016813/1, and the Swedish Research Council (VR) under Grant 2021-05842_VR..

REFERENCES

[1] Hsu, Cho-Kang, Chung, Shyh-Jong, "Compact Multiband Antenna for Handsets With a Conducting Edge.," IEEE Transactions on Antennas and Propagation, Vol.63, pp.5102–5107, 2015.

[2] Boukarkar, Abdelheq; Lin, Xian Qi; Jiang, Yuan; Yu, Yi Qiang, "Miniaturized Single-Feed Multiband Patch Antennas.," IEEE Transactions on Antennas and Propagation, Vol.65, pp.850–854, Feb. 2017.

[3] Lian, Ji-Wei; Ban, Yong-Ling; Zhu, Jia-Qi; Liu, Yanhui; Kang, Kai, "SIW Multibeam Antenna Based on Modified Horn Beam-Forming Network," IEEE Transactions on Antennas and Propagation Letter, vol. 17, no. 10, pp. 1866 – 1870, Oct. 2018.

[4] Li, Hui; Kang, Le; Wei, Feng; Cai, Yuan-Ming; Yin, Ying-Zeng, "A Low-Profile Dual-Polarized Microstrip Antenna Array for Dual-Mode OAM Applications," IEEE Transactions on Antennas and Propagation Letter, vol. 16, no. 16, pp. 3022 – 3025, Oct. 2017.

[5] Liu, Ying; Zhang, Wenbo; Jia, Yongtao; Wu, Anqi, "Low RCS Antenna Array With Reconfigurable Scattering Patterns Based on Digital Antenna Units," IEEE Transactions on Antennas and Propagation, vol. 69, no. 1, pp. 572 – 577, Jan. 2021.

[6] S. E. Mendhe and Y. P. Kosta, "Metamaterial properties and applications, " Int. J. Inf. Technol. Knowl. Manag., vol. 4, no. 1, pp. 85–89, 2011.

[7] D. Marathe and K. Kulat, "A compact triple-band negative permittivity metamaterial for C, X-band applications," International Journal Antennas Propagations, vol. 2017, pp. 1–12, 2017.

[8] P. Moitra, B. A. Slovick, W. Li, I. I. Kravchencko, D. P. Briggs, S. Krishnamurthy, and J. Valentine, "Large-scale all-dielectric metamaterial perfect reflectors," ACS Photon., vol. 2, no. 6, pp. 692–698, Jun. 2015.

[9] Somak Bhattacharyya, Devkinandan Chaurasiya, Kumar Vaibhav Srivastava, Anamiya Bhattacharya, and Saptarshi Ghosh, "Compact multi-band polarisation-insensitive metamaterial absorber," The Institute of Engineering and Technology Microwaves Antennas & Propagation, vol. 10, no. 1, pp. 94 – 101, January 2016.

[10] W. Kamonsin, P. Krachodnok, P. Chomtong, and P. Akkaraekthalin, "Dual-Band Metamaterial Based on Jerusalem Cross Structure With Interdigital Technique for LTE and WLAN Systems," IEEE Access, vol. 8, pp. 21565 - 21572, Jan. 2020.

[11] Ahdi Rezaeieh, S.; Antoniades, M. A.; Abbosh, A. M., "Gain Enhancement of Wideband Metamaterial-Loaded Loop Antenna With Tightly Coupled Arc-Shaped Directors," IEEE Antennas and Wireless Propagation, vol.65, Issue 4., pp. 2090–2095, Feb. 2017.

[12] B.A. Munk, Frequency-Selective Surface Theory and Design, Wiley Newyork,2000.

[13] R.V.S. Ram Krishna and R.Kumar, "Slotted ground microstrip antenna with FSS reflector for high-gain horizontal polarization," Electronics Letters, vol.51, no. 8, pp. 599-600, April 2015.

[14] Alfrêdo Gomes Neto, Jefferson Costa e Silva, Josiel Do Nascimento Cruz, João Batista de Oliveira Silva, and Nieremberg José Pereira de Lyra Ramos, "Multiband frequency selective surface with open matryoshka elements," 9th European Conference on Antennas and Propagation (EuCAP), April. 2015.

[15] Ahmed Abdelmottaleb Omar, and Zhongxiang Shen, "Multiband High-Order Bandstop 3-D Frequency-Selective Structures," IEEE Transactions on Antennas and Propagation, vol.64,Issue 6, pp. 2217–2226, March 2016.

[16] Ayan Chatterjee and Susanta Kumar Parui, "Frequency-Dependent Directive Radiation of Monopole-Dielectric Resonator Antenna Using a Conformal Frequency Selective Surface," IEEE Transactions on Antennas and Propagation, vol.65, pp. 2233–2239, May 2017.

[17] Li Yang; Mingyan Fan, Fanglu Chen, Jingzhao She, Zhenghe Feng, "A novel compact electromagnetic-bandgap (EBG) structure and its applications for microwave circuits," IEEE Transactions on Microwave Theory and Techniques, vol.53 , pp. 183–190, Jan.2005.

[18] Kamgaing, T.; Ramahi, O.M., "Multiband Electromagnetic-Bandgap Structures for Applications in Small Form-Factor Multichip Module Packages," IEEE Transactions on Microwave Theory and Techniques, vol.56 , pp. 2293–2300, Sep.2008.

[19] L. Li et al., "Surface-wave suppression band gap and planewavereflection phase band of mushroom-like photonic band gap structures," Journal of Applied Physics, vol. 130, No.2, pp. 1–8, 2008.

[20] Peng, Lin; Ruan, Cheng-li; Xiong, Jiang, "Compact EBG for Multi-Band Applications," IEEE Transactions on Antennas and Propagation, vol.60 , pp. 4440–4444, Sep.2012.

[21] Pandey, Ratnesh; Vishwakarma, Dinesh Kumar, "A meander line uniplanar EBG based multiband antenna using defected ground plane for WLAN and WiMAX applications," 2015 IEEE MTT-S International Microwave and RF Conference (IMaRC), No.15791055 , pp. 64–67, Dec.2015.

[22] Dewan, R.; Rahim, M.K.A.; Hamid, M.R.; Majid, H.A, "Multi band reconfigurable antenna using EBG unit cells," 2016 IEEE Asia-Pacific Conference on Applied Electromagnetics (APACE), No.16863994 , pp.38–42, Dec.2016.

[23] M. K. Abdulhameed et al., "Novel design of triple-band EBG," Telkomnika, vol. 17, no. 4, pp. 1682–4691, 2019.

[24] Yadav, Ajay; Goyal, Surabhi; Agrawal, Tanvi; Yadav, "Multiband antenna for Bluetooth/ZigBee/ Wi-Fi/WiMAX/WLAN/X-band applications Partial ground with periodic structures and EBG," Nature Communications, Vol.11 , No.4186, 21 August 2020.

[25] Zheng, Qi; Guo, Chenjiang; Vandenbosch, Guy A. E.; Ding, Jun, "Low-Profile Circularly Polarized Array With Gain Enhancement and RCS Reduction Using Polarization Conversion EBG Structures," IEEE Transactions on Antennas and Propagation, Vol.68 , pp.2440-2445, Oct. 2020.

[26] Prapoch Jirasakulporn, Pongsathorn Chomtong, Kamorn Bandudej, and Prayoot Akkaraekthalin, "A Compact Triple Band EBG Using Interdigital Coplanar Waveguide Structure for Antenna Gain Enhancement," International Journal of Antennas and Propagation, Vol.2020.

[27] Ahmed, Asif; Robel, Md. Rokunuzzaman, Rowe, Wayne S. T., "Dual-Band Two-Sided Beam Generation Utilizing an EBG-Based Periodically Modulated Metasurface," IEEE Transactions on Antennas and Propagation, Vol.68, Issue.4, Sep. 2020.

[28] Awais Khan, Shahid Bashir, Salman Ghafoor, and Khurram Karim Qureshi., "Mutual Coupling Reduction Using Ground Stub and EBG in a Compact Wideband MIMO-Antenna," IEEE Access, Vol.9, pp.40972-40979, March. 2021.

[29] Yanlin Hei, Min wang, Wen Wu, and Yizhou Wu., "A Fabry-Perot Cavity Antenna With Non-UniformSuperstrate and EBG Ground for High Gain and High Aperture Efficiency," IEEE Access, Vol.9, pp.101239-101245,July 2021.

[30] Anees Abbas, Niamat Hussain, Jaemin Lee, Seong Gyoon PARK, and Nam Kim, "Triple Rectangular Notch UWB Antenna Using EBG and SRR," IEEE Access, Vol.9, pp.2508-2515,Dec. 2021.

[31] Yu Guo, Haowei Wang, Sulei Fu, Shaoxu Dou, Weibiao Wang, and Haodong Wu, "Compact CEBG Filter for High-Frequency Applications With Low Insertion Loss," IEEE Transactions on Components, Packaging and Manufacturing Technology, Vol.13, No.1 pp.99-109, Jan. 2023.

[32] Dan Sievenpiper, Lijun Zhang, Romulo F. Jimenez Broas, Nicholas G. Alex´opolous, and Eli Yablonovitch, "High-Impedance Electromagnetic Surfaces with aForbidden Frequency Band," IEEE Transactions on Microwave and Techniques, Vol.47, No.11, Nov. 1999.

[33] Y Rhamat-Samil, and H Mosallaei,"Electromagnetic Band-Gap Structures Classification, Characterization and Applications," 11 th International Conference on Antennas and Propagation, No.480, April. 2001.

[34] Will Mckinzie, and Shawn Rogers,"A Multi-Band Artificial Magnetic Conductor Comprised of Multiple FSS Layer," IEEE International Symposium on Antennas and Propagation, No.03, pp.423-426, June. 2003.

[35] Douglas J. Kern, Douglas H. Werner, Agostino Monorchio, Luigi Lanuzza, and Michael J. Wilhelm, "The Design Synthesis of Multiband ArtificialMagnetic Conductors Using High Impedance Frequency Selective Surfaces," IEEE Transactions on Antennas and Propagation, Vol.53, No.1, Jan. 2005.

[36] Mª Elena de Cos, and Fernando Las-Heras, "Multi-band Artificial Magnetic Conductors with High Angular Stability," 7 th IEuropean Conference on Antenna and Propagation (EuCAP), pp.2510-2513, 2013.

[37] Alex Alvarado, Erik Agrell, Domanic¸ Lavery, Robert Maher, and Polina Bayvel., "Replacing the Soft-Decision FEC Limit Paradigm in the Design of Optical Communication Systems," Journal of Lightwave Technology, Vol.33, No.20, OCT. 2015.

[38] Nader Engheta, and Richard W Ziolkowski., "Metamaterials Physics and Engineering Explorations," Wiley-IEEE Press, 2006.

[39] Fan Yang, and Yahya Rahmat-Samii., "Electromagnetic Band Gap Structures in Antenna Engineering," Cambridge University Press, OCT. 2008.

[40] Li, Yading., "Investigation of minimum cavity height of small EBG-resonator antennas for maximum directivity,"2009 Asia Pacific Microwave Conference, Dec.2009.

[41] J. Coonrod, "Comparing micostrip and CPW performance," Microwave Journal, vol. 55, no. 7, pp. 74–82, 2012.

[42] M. E. de Cos and F. Las-Heras, "Dual-band uniplanar CPW fed monopole/EBG combination with bandwidth enhancement,"IEEE Antennas and Wireless Propagation Letters,vol. 11, pp. 365–368, 2012.

[43] M. Joodaki and M. Rezaee, "Coplanar waveguide (CPW) loaded with electromagnetic band gap (EBG) structuremodeling and application to displacement sensor," IEEE Sensors Journal, vol. 16, no. 9, 2016.

[44] Rainee N.Simons, "Coplanar Waveguide Circuits, Components and Systems," John Wiley&Son, 2001

[45] F. Xu, L. Li, K. Wu, S. Delprat, and M.Chaker,"Parameterextraction of interdigital slow-wave coplanarwaveguide circuitsusing finite difference frequency domain algorithm,"International Journal of RF and Microwave Computer-AidedEngineering, vol. 18, no. 3, pp. 250–259, 2008.

[46] Xu, F.-L., Liu, X.-G., Guo, H.-P., et al., "A compact dual modeBPF based on interdigital structure." IEEE Microwave and Millimeter Wave Technology International Conference (ICMMT), pp. 1595–1597, 2010.

[47] S. Meesomklin, P. Chomtong, and P. Akkaraekthalin, "A compact multiband bpf using step-impedance resonators with interdigital capacitors," Radioengineering, vol. 25, no. 2, pp. 258–267, 2016.

[48] R. S. Beeresha, A. M. Khan and R. H. V. Manjunath, "Design and optimization of interdigital capacitor," ICRIET-2016, pp.73-78, Nov. 2016.

[49] B. Belyaev, A. M. Serzhantov, A. A. Leksikov, Y. F. Bal'va, and A. A. Leksikov, "High-Quality Compact Interdigital Microstrip Resonator and Its Application To Bandpass Filter," Prog. he Electromagn. Res. C, vol. 72, Oct. 2016, pp. 91–103, 2017.

[50] R. S. Beeresha, A. M. Khan and R. H. V. Manjunath, "Design and optimization of interdigital capacitor," ICRIET-2016, pp.73-78, Nov. 2016.

[51] Paris Vélez, Jordi Selga, Jordi Bonache and Ferran Martín, "Slow-wave inductively-loaded electromagnetic bandgap (EBG) coplanar waveguide (CPW) transmission lines and application to compact power dividers," 46th European Microwave Conference (EuMC), pp 104-107, 2016.

[52] T.Zhou, Y. Cao and Z. Cheng, "Compact multiband interdigital-coupled-fed planar antenna with stepped-impedance structure for mobile handsets," Hindawi, International journal ot antennas and propagation, vol. 2017, 2017.

P. CHOMTONG (Member, IEEE) He received his M.Eng. and Ph.D. degrees in Electrical Engineering from King Mongkut's University of Technology North Bangkok (KMUTNB), Thailand, in 2006 and 2011, respectively. In 2012, he joined the Department of Teacher Training in Electrical Engineering, KMUTNB, as an instructor. His current research interests include passive and active microwave circuits, wideband and multiband antennas, and telecommunication systems. He is a member of IEEE.

P. KRACHODNOK (Member, IEEE) received the M. Eng. degree in Electrical Engineering from Chulalongkorn University (CU), Thailand, in 2001, and the Ph.D. degree in telecommunication engineering from the Suranaree University of Technology (SUT), Thailand, in 2008. Since 2001, she has been with the School of Telecommunication Engineering, SUT. She has experience and an expert in electromagnetic theory, microwave engineering, and antenna engineering.

J. Konpang (Member, IEEE) He received the M.Eng. from the King Mongkut's University of Technology North Bangkok (KMUTNB), Thailand, in 2004, and the PhD. Degree in electronic and electrical engineering from the university of Leeds, UK, in 2018. In 2021, he was appointed as a Lecturer (Associate Professor) with the department of electrical and telecommunication engineering at Rajamangala University of Technology Krungthep. Now, his main research focuses on electric vehicle and microwave engineering.

N. Somjit (Senior Member, IEEE) received the Dipl.-Ing. (M.Sc.) degree from the Dresden University of Technology, Dresden, Germany, in 2005, and the Ph.D. degree from the KTH Royal Institute of Technology, Stockholm, Sweden, in 2012. Then, he returned to TU Dresden to lead a research team in microsensors and MEMS ICs for the Chair for Circuit Design and Network Theory. In 2013, he was appointed as a Lecturer (Assistant Professor) with the School of Electronic and Electrical Engineering, University of Leeds, Leeds, U.K., where he is currently an Associate Professor. Since 2022, he has been appointed to lead a research team as an Adjunct Faculty Member in Micro and Nanosystems Department, KTH Royal Institute of Technology. His main research focuses on integrated smart high-frequency components, sustainable micro and nanosystems, and low-cost microfabrication processes.Dr Somjit was appointed as a member of the Engineering, Physical and Space Science Research Panel of the British Council in 2014. He was a recipient of the Best Paper Award (EuMIC Prize) at the European Microwave Week in 2009. He was awarded the Graduate Fellowship from the IEEE Microwave Theory and Techniques Society (MTT-S) in 2010 and 2011, and the IEEE Doctoral Research Award from the IEEE Antennas and Propagation Society in 2012. In 2016, he was the Chair of the Student Design Competition for the European Microwave Week and, in 2018, he was appointed as an Associate Editor of IET Electronics Letters.

C. **MAHATTHANAJATUPHAT** (Member, IEEE) received the M.Eng. degree from the University of Applied Sciences Rosenheim, Germany, in 2003, and the Ph.D. degree from the King Mongkut's University of Technology North Bangkok (KMUTNB), Thailand, in 2009. In 2017, he was appointed as a Lecturer (Associate Professor) at the Department of Electrical Engineering, KMUTNB. His main research interests include the designing of small antennas using the fractal geometry and digital signal processing for communication applications.

P. AKKARAEKTHALIN (Member, IEEE) He received the B.Eng. and M.Eng. degrees in Electrical Engineering from King Mongkut's University of Technology North Bangkok (KMUTNB), Thailand, in 1986 and 1990, respectively, and the Ph.D. degree from the University of Delaware, Newark, USA, in 1998. From 1986 to 1988, he worked in the Microtek Laboratory, Thailand. In 1988, he joined the Department of Electrical Engineering, KMUTNB. His current research interests include passive and active microwave circuits, wideband and multiband antennas, and telecommunication systems. Dr. Prayoot is members of IEEE, IEICE Japan, and ECTI Thailand. He was the Chairperson for the IEEE MTT/AP/ED Thailand Joint Chapter during 2007 and 2008 and the President of ECTI Association from 2014 to 2015. He is now the head for Senior Research Scholar Project of Thailand Research Fund (TRF).